Raman study of the surface oxidation in (U, Pu)O_2 as a function of Pu content

Jone Miren Elorrieta, Dario Manara, Laura Jiménez Bonales, Jean-François Vigier, Oliver Dieste, Mohamed Naji, Renaud C. Belin, Valentín García Baonza, Rudy Konings, Joaquín Cobos

Raman study of the oxidation in (U, Pu)O_2 as a function of Pu content

J.M. Elorrieta [a, *], D. Manara [b], L.J. Bonales [a], J.F. Vigier [b], O. Dieste [b], M. Naji [b], R.C. Belin [c], V.G. Baonza [d], R.J.M. Konings [b], J. Cobos [a]

[a] Centro de Investigaciones Energéticas, Medioambientales y Tecnológicas, CIEMAT, Avenida Complutense 40, 28040 Madrid, Spain
[b] European Commission, Joint Research Centre (JRC), Postfach 2340, 76125 Karlsruhe, Germany
[c] CEA, DEN, DEC, SESC, LLCC, Cadarache, F-13108 Saint-Paul-Lez-Durance, France
[d] MALTA-Consolider Team, Departamento de Química Física I, Facultad de Ciencias Químicas, Universidad Complutense, 28040 Madrid, Spain

This work presents a systematic Raman study of the matrix oxidation in a variety of (U_{1-y}, Pu)O_2 compositions ($0 \leq y \leq 0.46$) at different temperatures, between 250 °C and 400 °C. Our results indicate that the increase in Pu content hinders the oxidation process of the dioxide matrix. Further oxidation of the uranium-plutonium mixed dioxides in air starts between 250 °C and 310 °C, on a time scale of several hours. M_4O_9 seems to be the most stable intermediate phase formed upon oxidation of all the investigated mixed oxides, before final oxidation to M_3O_8. In addition, X-ray diffraction measurements and SEM images confirm the trend observed by Raman spectroscopy, *i.e.* Pu stabilises the fcc structure of the dioxide.

1. Introduction

The performance assessment of spent nuclear fuel (SNF) stability under dry interim storage conditions is of great importance in nuclear waste technology. In case of failure of the engineered containment barriers, oxidation of the spent fuel matrix (UO_2) might take place depending on the oxygen concentration in the surroundings and the temperature produced by the decay heat. As is well known, oxidation of UO_2 to U_3O_8 involves an increase in volume of around 36% that might affect fuel integrity and, consequently, storage safety [1]. Hence, it becomes necessary to understand in detail how this reaction proceeds, analysing step-by-step not only the different uranium oxides that take part in the oxidation, but also the reaction mechanisms responsible for the consecutive structural transitions along the $UO_2 \rightarrow U_4O_9/U_3O_7 \rightarrow U_3O_8$ transformation [2].

In particular, the first stage of the latter reaction, *i.e.* UO_2 evolution to U_4O_9/U_3O_7, takes on special interest owing to the fact that various crystal symmetry transitions occur along this compositional range while the overall structure remains cubic [3]. Such transitions have been experimentally detected by means of Raman spectroscopy and X-ray diffraction (XRD) [4,5]. As additional oxygen atoms are incorporated into the *Fm-3m* cubic lattice, they continuously rearrange without altering it in a significant way, eventually giving rise to a so-called superstructure. This corresponds to the U_4O_9 phase, which consists of a very densely packed cubic structure where oxygen atoms arrange themselves into cuboctahedral clusters [6]. Likewise, U_3O_7 has a distorted cubic lattice, only differing from U_4O_9 in the slight alteration caused by the excess of oxygen [3].

* Corresponding author. Centro de Investigaciones Energéticas, Medioambientales y Tecnológicas, CIEMAT, Departamento de Energía, Unidad de Residuos de Alta Actividad, Av. Complutense 40, 28040 Madrid, Spain.
E-mail address: jonemiren.elorrieta@ciemat.es (J.M. Elorrieta).

Full comprehension of this oxidation reaction becomes even a greater challenge when, instead of dealing with pure uranium dioxide, it concerns uranium-based mixed oxides like (U, Pu)O_2, commonly referred to as MOX, and (U, Am)O_{2-x}. Such is the case of the potential fuels for fast neutron reactors, mainly intended for nuclear waste radiotoxicity reduction. In this sense, it is certainly necessary to assess the behaviour of the transuranium elements within the UO_2 matrix and their influence in the stability of this kind of SNF against oxidation/corrosion during storage.

Especially, the effect of Pu incorporation into the UO_2 matrix has been frequently addressed, since MOX fuels have been used for at least 30 years in some countries, *e.g.* France, Belgium or Germany, with the aim of recycling Pu in Light Water (thermal) Reactors (LWR) [7]. In this way, (U_{1-y}, Pu_y)O_2 oxides with different *y* values as well as a few spent MOX fuels have been characterised and their oxidation in some cases investigated [8–21]. In these studies, a variety of experimental techniques have been employed, although XRD is by far the most frequent. Already in the 1970s, XRD measurements were applied for analysing the oxidation products of uranium-plutonium mixed oxides obtained in a thermal balance [8,9]. More recently, the effect of Pu content on the mixed dioxide lattice parameter at room temperature and the structure evolution after oxidation have been assessed [10–17]. In all of them the lattice parameter has been reported to follow Vegard's law, decreasing linearly as a function of plutonium concentration. With regard to oxidation of (U_{1-y}, Pu_y)O_2 oxides at different temperatures, it has been found that Pu stabilises the cubic phase during the reaction and that the temperature of M_3O_8 formation is higher as Pu content increases [15].

Furthermore, Raman spectroscopy of nuclear materials and actinide compounds has been broadly developed in the last decade [4,5,18–34]. This is not only due to advances in Raman spectroscopy approaches, their versatility, and potential non-contact analyses, but also to the improvement of confinement techniques for highly radioactive materials [21,30,31], which have allowed the study of hazardous compounds practically unexplored until the last decade of the Twentieth Century.

Concerning uranium-plutonium mixed oxides, certain studies have provided Raman characterisation of both unirradiated samples and spent fuels corresponding to different Pu contents [18–22]. A higher oxidation resistance of this kind of mixed dioxides as Pu concentration increases has also been reported [20,21].

Nevertheless, none of these studies has systematically evaluated, directly by Raman spectroscopy, the matrix oxidation of (U, Pu)O_2 mixed oxides under different temperature conditions and as a function of Pu content. Such a detailed Raman analysis of the matrix oxidation, within a varying range of Pu concentrations, is presented here for the first time.

2. Experimental

2.1. Materials

A variety of starting (U_{1-y}, Pu_y)O_2 fragments, averaging 1-3 mm in surface size, with different Pu contents ranging from $y = 0$ up to $y = 0.46$ were used in this work. Some of them were provided by CEA (Commissariat à l'Energie Atomique, France) and others by JRC-Karlsruhe (Joint Research Centre, Germany). CEA samples were prepared and characterised by a well established powder metallurgy procedure described in previous publications [17]. JRC samples were prepared by sintering powders produced by sol-gel technique, as described elsewhere [22]. Table 1 comprises data concerning the samples, such as the *MOX* reference utilised hereafter for each one, the proportion of Pu they contain and their provider.

Table 1
List of (U, Pu)O_2 mixed oxides used in this work.

Reference	Pu Content (mol%) (±2)	Provider
UO_2	0	JRC
MOX 3.7	3.7	JRC
MOX 14	14	CEA
MOX 19	19	CEA
MOX 35	35	CEA
MOX 46	46	CEA

2.2. Sample preparation

Starting samples listed in Table 1 were annealed at 1600 °C during 15 min under reducing conditions (Ar + 6.5% H_2 flow), enabling the removal of lattice defects expected from alpha self-irradiation. Thereafter, the oxidation procedure consisted in heating them at a constant rate of 10 °C/min up to a given temperature in each experiment, *i.e.* 250, 310, 340 and 400 °C, under a synthetic air flow and maintaining the selected temperature for 3 h. The samples were withdrawn immediately after this time period elapsed, with the aim of avoiding further oxidation due to the slow inertial cooling of the furnace tube. Both annealing and oxidation experiments were carried out in an alumina tube furnace.

2.3. Raman spectroscopy

Due to the radioactivity of the MOX samples, it was necessary to encapsulate them prior to Raman spectra measurements into α-shielding Plexiglas capsules recently designed and developed by JRC-Karlsruhe [31]. The spectra were recorded through the quartz window on top of these capsules.

Raman measurements were performed with a Jobin-Yvon T 64000 spectrometer. All spectra were acquired at an excitation wavelength of 647 nm, provided by a Kr^+ laser. The laser beam was focused on the sample through a long focal distance objective (NA (*Numerical Aperture*) = 0.5) with 50× magnification. The excitation power was optimised between 50 and 100 mW (being around 5 times lower at the sample surface [29]) in order to prevent further oxidation of the samples by the laser. The scattered radiation was dispersed using a 1800 grooves/mm holographic grating and recorded by a liquid-nitrogen cooled CCD detector. The single spectrograph configuration applied enabled a spectral resolution of ±1 cm^{-1}. The spectrometer was daily calibrated using the T_{2g} phonon (520.5 cm^{-1}) of a silicon single crystal [35].

2.4. X-ray diffraction

XRD analyses were performed on crushed samples. About 20 mg of powder were loaded in an epoxy resin to avoid excessive dispersion of radioactive powder. A Seifert XRD-3003 X-ray diffractometer (Cu Kα radiation) with a Bragg-Brentano θ/θ configuration was used for the analyses. The device is implemented in a glove-box for radioactive material confinement. The powder patterns were recorded using a step size of 0.02° across the angular range $10° \leq 2\theta \leq 120°$. Structural analyses were performed by the Rietveld method using Jana2006 software [36]. Peak-profile analysis was carried out using pseudo-Voigt bandshapes.

2.5. Scanning electron microscopy

The scanning electron microscopy used in this work is a Philips XL40 SEM (Philips, Amsterdam, Netherlands), which has been modified in order to be used for the examination of highly active or irradiated nuclear materials [37,38]: the chamber, column,

turbomolecular pump and the high voltage unit are mounted inside a glove-box in order to keep the contamination in a confined space, whereas the primary vacuum system, water cooling circuit and acquisition electronics are placed outside, provided those parts are not contaminated by the active samples, thus facilitating the equipment mantainance. The microscope is equipped with Secondary-electron detector (SE) which gives a morphology-related signal, Backscattered-electron detector (BSE) which provides images with Z-related contrast, and Energy dispersive X-ray spectroscopy (EDS) used to obtain elemental analysis of the samples. The beam was operated during this work at 25 kV.

3. Results and discussion

3.1. Initial characterisation

XRD and X-ray absorption spectroscopy (XAS) characterisation of the samples was performed on as-fabricated materials. Both their composition and the attainment of single phase materials were confirmed, based on XRD. The results of these characterisation campaigns are published in previous papers [15,22].

Prior to conducting the different oxidising heat treatments, Raman spectra of each annealed MOX sample were acquired, as shown in Fig. 1. UO_2 spectrum features two characteristic bands at about 445 and 1150 cm^{-1}, which are well known and correspond to the T_{2g} mode [39] and the 2LO phonon overtone [40], respectively. Inasmuch as Pu content increases, the general aspect of the spectra changes: a) the T_{2g} band shifts continuously to higher wavenumbers, b) the 2LO band diminishes until it is no longer discernible, c) a broad band appears at 500-600 cm^{-1} (labelled with a rhombus), and d) another feature is observed around 850-1000 cm^{-1}.

The continuous shift to higher wavenumbers of the T_{2g} band with the increase of Pu content is caused by the shortening of the M(U,Pu)-O bonds [20]. The up-shift in the T_{2g} mode is essentially linear, ranging from around 445 cm^{-1} for pure UO_2 to 478 cm^{-1} for pure PuO_2 [4,22,24,25,29,30,39–44]. Both the attenuation of the 2LO peak and the appearance of a new band *ca.* 500-600 cm^{-1} can

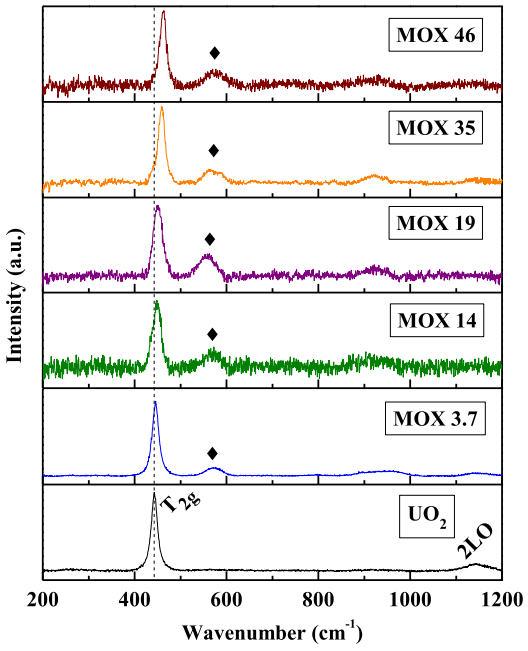

Fig. 1. Raman spectra of the initial $(U_{1-y}, Pu_y)O_2$ samples, with $0 \leq y \leq 0.46$.

be associated with lattice distortions (non-perfect fluorite structure) [4,27,42,44], due in this case to the partial substitution of U atoms by Pu atoms. The simultaneous presence of Pu^{3+} and U^{5+} cations, already observed in this kind of compounds for example by X-ray absorption spectroscopy [22], might in fact foster the formation of Frenkel-like defects, which have been proposed to be responsible for an analogue spectral feature found around 575 cm^{-1} in UO_2 [45] and at ~578 cm^{-1} in PuO_2 [29]. The broad band at 850-1000 cm^{-1} might be related to the first overtone of the T_{2g} mode of PuO_2 [29,46]. Slight differences in the intensity ratios of some bands when comparing with previous studies [19,20] may be attributed to the different excitation wavelength used in this work [3].

A second derivative analysis [47] was applied to every spectrum with the aim of determining the position of the T_{2g} band more accurately for each MOX sample. The approximately linear behaviour of the T_{2g} position as a function of Pu content in the mixed oxides (Fig. 2a) reflects the correct estimation of the Pu content value for all the samples, assuming a one-mode T_{2g} vibration [48]. This one-mode model assumption, already reported in previous studies [19,20,22], was confirmed by fitting the T_{2g} band and ascertaining a single-peak contribution. Fig. 2b shows these peak fitting results in the case of MOX 46, where a two-mode behaviour should be noticeable (if existing), but a sole peak is likewise observed. T_{2g} positions are also in good agreement with those reported by Böhler et al. [22].

3.2. Behaviour under different temperature conditions

3.2.1. Raman analysis

Following every oxidising heat treatment, characterisation of the treated MOX samples was carried out by Raman spectroscopy. Fig. 3 compiles the recorded spectra, organised on the basis of the temperature maintained in each experiment (250, 310, 340 and 400 °C). A few spectra are missing due to lack or damage of certain samples when the measurements were performed.

Fig. 3a shows that the spectra of those oxides subjected to 250 °C remained almost unaltered, featuring essentially the same bands as the initial samples: T_{2g} and 2LO bands in the case of UO_2, and T_{2g} and 500-600 cm^{-1} bands (marked again with a rhombus) for MOX samples. This suggests that no significant oxidation occurred, at least within the Raman laser penetration depth scale, which is estimated to be around 500 nm for our set-up and materials. However, a slight superficial oxidation seems to have taken place, as pointed out by: 1) an appreciable symmetry loss of the T_{2g} band-shape and the appearance of a very broad feature around 700-800 cm^{-1} (characteristic of U_3O_8) in the UO_2 spectrum, and 2) the slight T_{2g} shift detected for those MOX samples with the lowest Pu content (particularly in MOX 3.7).

On the other hand, results obtained for the treatments at higher temperatures (Fig. 3b-d) indicate that all samples were oxidised to a greater or lesser extent. Indeed, apart from UO_2, where traces of U_3O_8 could also be deduced from an additional band detected around 800 cm^{-1}, the M_4O_9 phase was found to be stable in all the compositions after 3 h at 310 °C (Fig. 3b). The sole presence of a remarkably shifted T_{2g} mode and a broad and asymmetric band at around 630 cm^{-1} was previously assigned to U_4O_9 [3]. Likewise, this shifted and broadened T_{2g} band and a wide feature observed around 640-645 cm^{-1} have been recently associated with the M_4O_9 phase when oxidizing both an aged MOX 24 and an agglomerate (with about 20% Pu content) of a spent MOX fuel under the laser beam [19,21]. The same two features can be observed in every spectrum of Fig. 3b, where an asterisk marks the appearance of the *ca.* 640 cm^{-1} band. It should be noted that the 500-600 cm^{-1} band is no longer observed, what might suggest the disappearance of

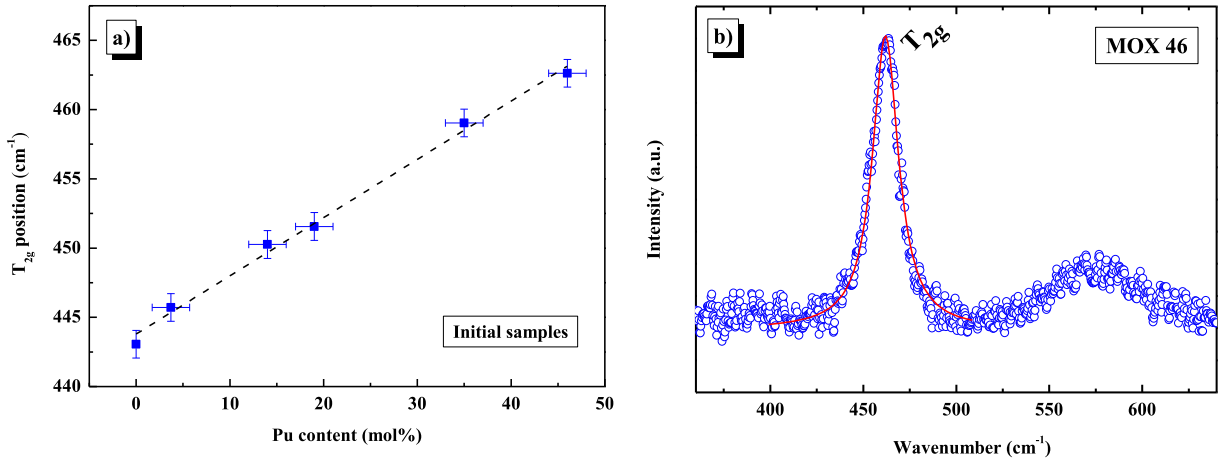

Fig. 2. a) Position of the T_{2g} band vs. Pu content of the different MOX samples. b) Peak fitting performed on the T_{2g} band of MOX 46 Raman spectrum.

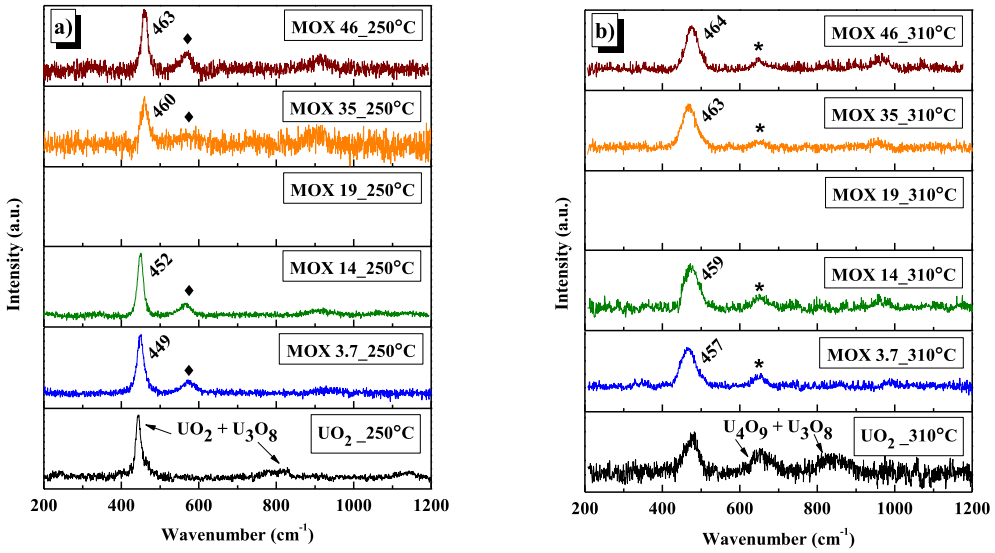

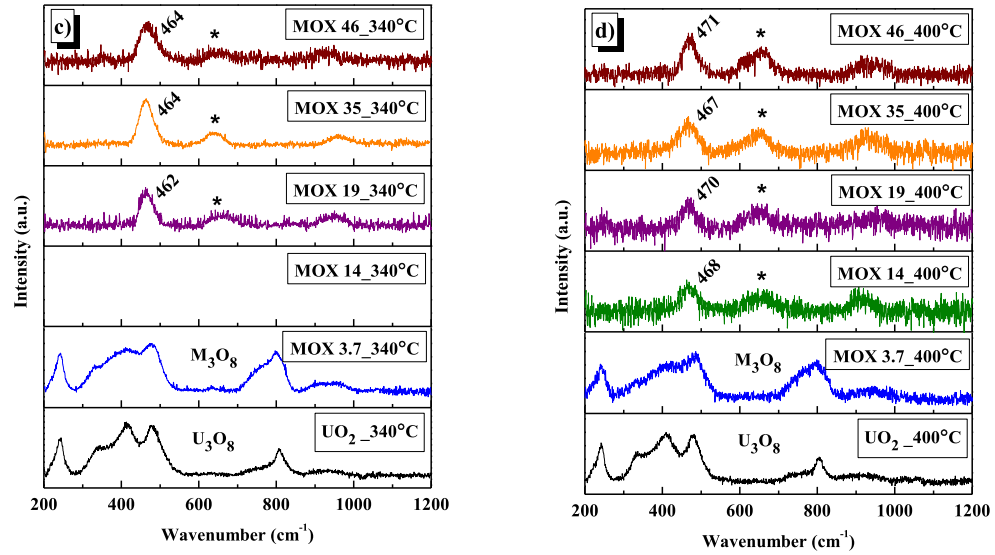

Fig. 3. Raman spectra of $(U_{1-y}, Pu_y)O_2$ oxides, with $0 \leq y \leq 46$, after 3 h heat treatments at a) 250 °C, b) 310 °C, c) 340 °C and d) 400 °C under a synthetic air flow. Blank spaces correspond to missing spectra (due to lack or damage of certain samples when the measurements were performed) and have not been removed for the sake of clarity.

Frenkel-like defects and thus the formation of M_4O_9 as a new ordered structure where even the defects manage to rearrange.

With regard to the other two treatments at higher temperatures (Fig. 3c and d), M_4O_9 was again the predominant phase, and the T_{2g} band for each MOX composition was found to be more shifted to higher wavenumbers as temperature increased. In this case, the exceptions were UO_2 and the MOX oxide with the lowest Pu concentration (*i.e.* MOX 3.7), which showed complete oxidation to M_3O_8 after the 340 °C (Fig. 3c) and the 400 °C (Fig. 3d) treatments. Conversion to M_3O_8 can be easily distinguished, owing to the appearance of several bands located at around 236, 342, 408, 480, 752 and 798 cm^{-1} [41,49]. The intensity of the 752 cm^{-1} line seems to be higher and the 342-480 cm^{-1} bands not so clearly defined for those oxides containing plutonium than for pure U_3O_8. No reference about this observation has been made in the literature before, to the best of our knowledge. In addition, a slight contribution can be detected around 800 cm^{-1} in the spectra of those MOX oxides that were not completely converted to M_3O_8 after the 400 °C treatment, especially MOX 14 and MOX 19 (Fig. 3d). This might point out a minor presence of the M_3O_8 phase, although the low signal-to-noise ratio of these spectra makes it difficult to clearly assess such possibility.

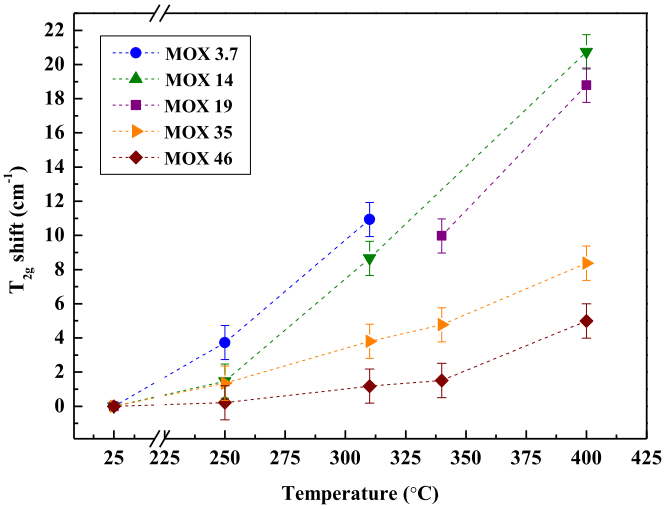

Fig. 4. T_{2g} shift of the partially oxidised $(U_{1-y}, Pu_y)O_2$ samples ($0.037 \leq y \leq 0.46$) with respect to their initial position, as a function of the heat treatment temperature.

All the latter results indicate that the main phase transitions ($MO_2 \rightarrow M_4O_9 \rightarrow M_3O_8$) of the uranium-plutonium mixed dioxides take place in air between 250 °C and 310 °C (on a time scale of several hours) and that, as previously quoted [1], Pu content plays a significant role with regard to the fcc dioxide matrix preservation. In every heat treatment the M_4O_9 phase seems to be stabilised for high Pu content samples, hence preventing, in overall terms, further oxidation to M_3O_8. Besides, the shift in the T_{2g} mode of each partially oxidised MOX sample with respect to its initial T_{2g} position, due to oxygen incorporation into the fluorite lattice [4,5], is less significant as the Pu proportion increases (Fig. 4), what points out that a higher Pu content also helps to slow down the dioxide matrix oxidation.

3.2.2. XRD measurements

Due to the small quantity (some mg) of the current MOX samples available, it was possible to perform a post-heat treatment powder XRD analysis only on a few of them. The results are shown in Fig. 5.

One can see in the lattice parameter vs. composition graph of Fig. 5b that the formation of new oxides with O/M > 2 occurs in UO_2-richer compositions heat-treated in air. This is signified by the fact that lattice parameters of fluorite-like phases heat treated in air at 310 °C are slightly, but systematically, below the values predicted by Vergard's law—except for MOX 46—(see Table 2 for further detail) [52]. This effect is larger the lower the Pu content, confirming that a higher oxidation takes place in U-richer samples. The only XRD measurement performed on a MOX sample treated at 400 °C (MOX 19) clearly shows a much greater deviation with respect to Vegard's-law prediction in lattice parameter, as well as a large segregation of a M_3O_8 phase ($(U,Pu)_3O_8$ in Fig. 5a). Raman results are therefore qualitatively corroborated by XRD analyses. Since powder XRD is essentially a bulk characterisation technique,

Table 2
Experimental and predicted (from Vegard's law for stoichiometric samples) lattice parameter values of the measured MOX oxides.

Sample	Heat Treatment Applied	Experimental Lattice Parameter (Å)	Vegard's Law Predicted Lattice Parameter (Å)
MOX 3.7	3 h at 310 °C	5.465(1)	5.468(1)
MOX 19	3 h at 310 °C	5.454(1)	5.457(1)
MOX 19	3 h at 400 °C	5.426(1)	5.457(1)
MOX 35	3 h at 310 °C	5.443(1)	5.445(1)
MOX 46	3 h at 310 °C	5.438(1)	5.437(1)

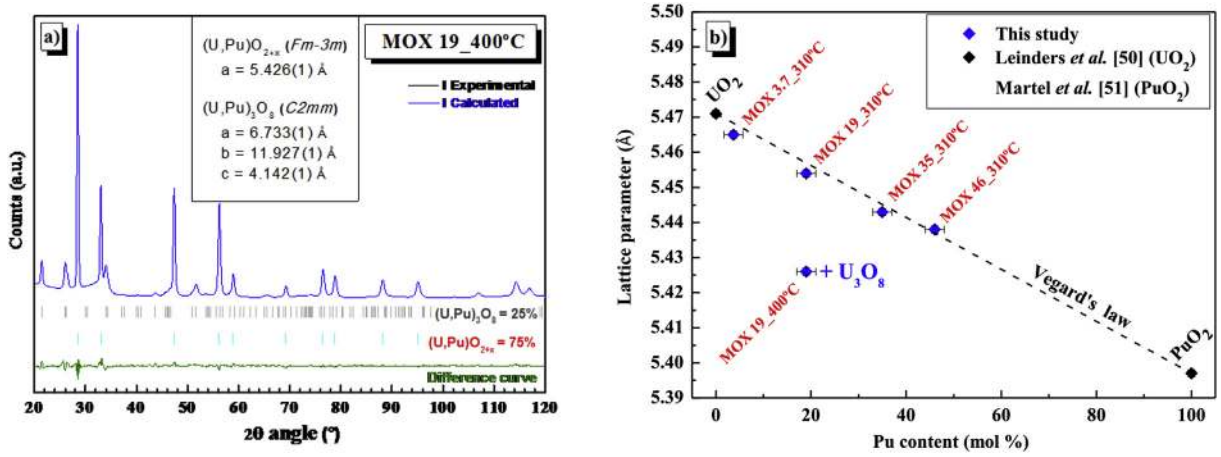

Fig. 5. a) X-ray diffraction pattern of MOX 19 after the 400 °C heat treatment. b) Lattice parameters obtained for all the measured MOX samples, as a function of Pu content. The dashed line represents values predicted by Vegard's law, taking as a reference UO_2 and PuO_2 experimental lattice parameters [50,51].

the agreement between XRD and Raman results also confirms that the current Raman data are representative of a bulk oxidation behaviour, and not just for the "deep surface".

3.2.3. SEM images

SEM images were acquired for a variety of MOX samples treated at 250 °C (Fig. 6) and 400 °C (Fig. 7), in order to qualitatively investigate the crystal grain morphology and correlate it to Raman and XRD results. Fig. 6 shows that grains in both MOX 3.7 and MOX 46 are large (≥10 μm) and regular after the 250 °C heat treatment, suggesting that no significant microstructural evolution has taken place, in good agreement with Raman results. Nevertheless, MOX 3.7 grains seem to be slightly swollen (see pores surroundings in Fig. 6a), what might be

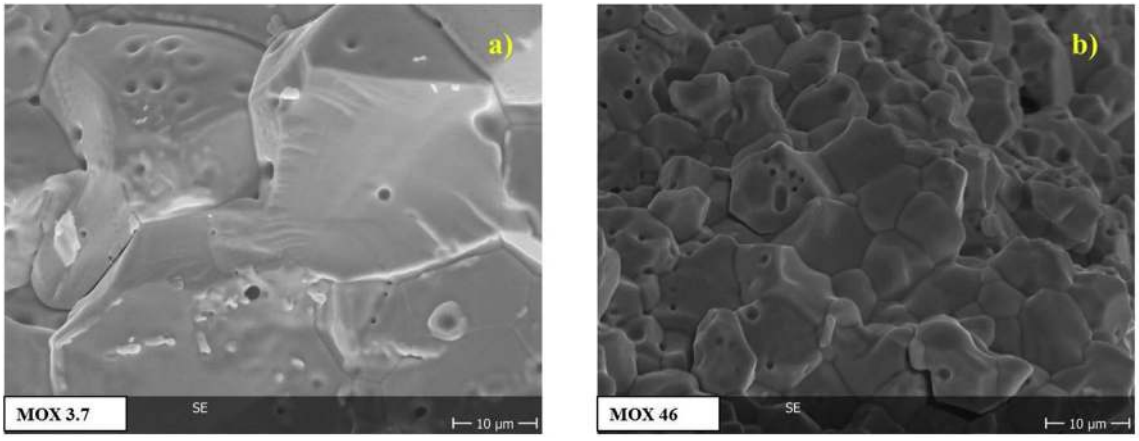

Fig. 6. SEM images obtained for a) MOX 3 and b) MOX 46, after the 250 °C heat treatment.

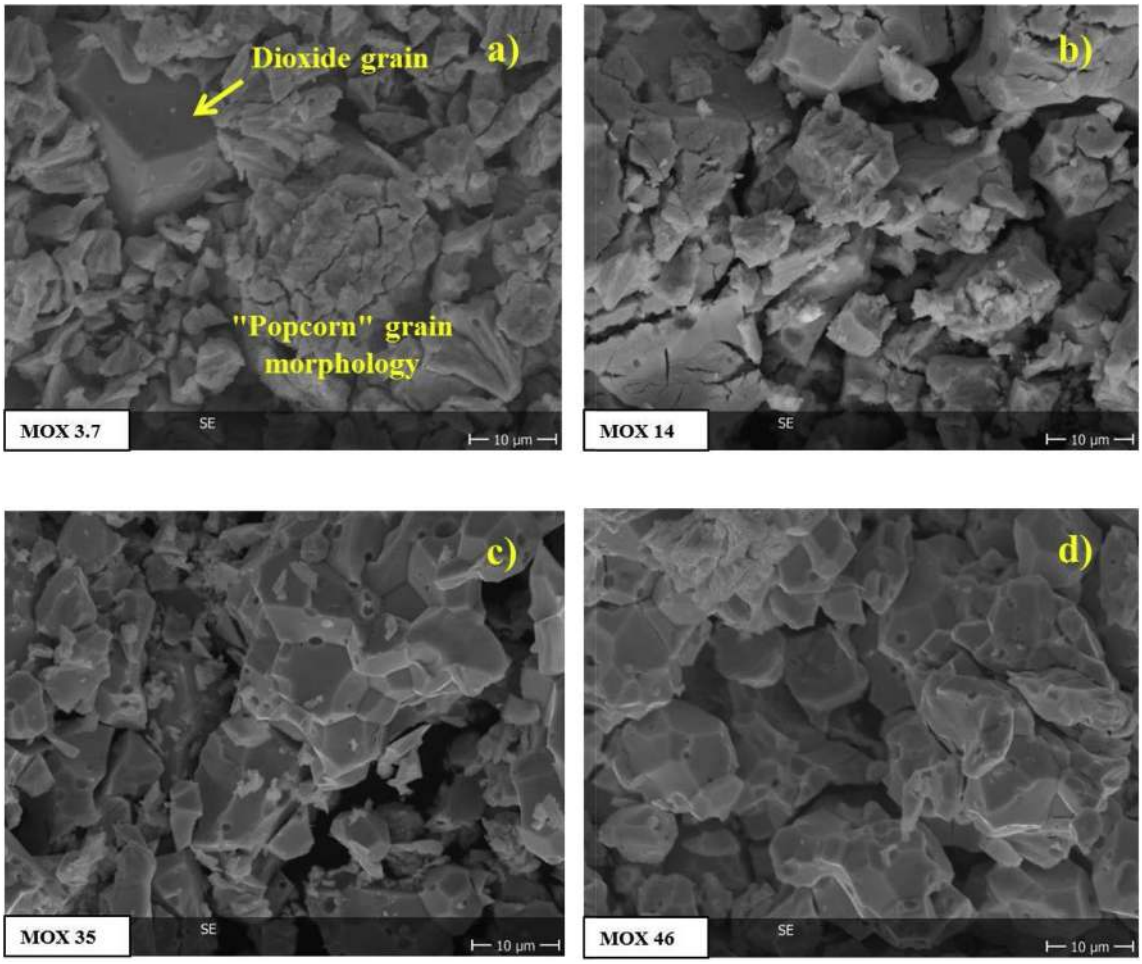

Fig. 7. SEM images obtained for a) MOX 3, b) MOX 14, c) MOX 35 and d) MOX 46, after the 400 °C heat treatment.

ascribed to the minor superficial oxidation previously noticed by Raman spectroscopy for this sample.

On the other hand, the sequence of images presented in Fig. 7 fairly depicts the hindering effect of Pu on the dioxide matrix oxidation, as observed by Raman and XRD. After subjecting them to 400 °C during 3 h, each MOX sample exhibits a different surface aspect. If one compares Fig. 7a with Fig. 6a, it is evident that larger - most likely cubic-grains of MOX 3.7 appear to be covered by a superficial layer of M_3O_8, commonly associated with a so-called "popcorn" effect [1]. A similar popcorn morphology can be partly seen also in MOX 14 (Fig. 7b), which also shows considerably swollen and cracked grains (both inter and intragranularly). MOX 35 presents intergranular cracking only, with some swollen areas located in the openings originated by this effect. MOX 46 looks similar to MOX 35, although with a more compact aspect, indicating a lower loss of integrity might have taken place.

This qualitative analysis of the crystal grain aspect in various MOX samples shows an evolution of the sample surface morphology, which is in line with the trend derived from Raman spectroscopy analyses, *i.e.* the lower the Pu content, the larger the oxidation effects.

4. Conclusions

The surface oxidation of the matrix in a variety of uranium-plutonium mixed dioxides has been analysed by Raman spectroscopy under different temperature conditions, thereby assessing the effect of Pu content.

In the case of MOX samples subjected to 250 °C during 3 h, no significant oxidation has been observed in any of the Raman spectra, except for the slight appearance of U_3O_8 traces in pure UO_2. Higher temperatures are needed in order to trigger appreciable chemical reactions between oxygen and the present samples. However, for all other heat treatments (310, 340 and 400 °C) oxidation does occur and the obtained data point out that a higher proportion of Pu slows down the dioxide matrix oxidation. In fact, M_4O_9 is observed as the intermediate stable phase in every MOX sample before oxidising to M_3O_8. XRD measurements and SEM images are in good agreement with Raman results, confirming the stabilising effect of Pu^{4+} on the fcc dioxide structure.

The present study therefore shows, with the sole help of Raman spectroscopy, that (U, Pu) mixed dioxides are subject to further oxidation in air starting at a temperature between 250 °C and 310 °C, at least on a time scale of several hours.

In any case, this work demonstrates that Raman spectroscopy is highly reliable for evaluating the uranium-plutonium dioxide fuel oxidation, since its transformation to M_4O_9 or M_3O_8 can be easily and quickly monitored with this technique.

In addition, thanks also to its instrinsically non-contact nature and versatility, Raman spectroscopy can be envisaged as a suitable technique for the analysis of the oxidation behaviour of spent nuclear fuel, in case of shielding failure, under interim storage conditions.

Acknowledgements

This work was carried out within the collaboration framework established between CIEMAT and EC-JRC Karlsruhe (Collaboration Agreement Nº 34231 and User Access Agreement Nº 930009), and supported by the Graduate and Executive Nuclear Training and Longlife Education (GENTLE) project (EURATOM FP7 contract number 323304). The authors are indebted to J.-Y. Colle, M. Sierig and E. Dahms (JRC-Karlsruhe) for their help in the samples characterisation and the Raman measurements.

References

[1] R.J. McEachern, P. Taylor, J. Nucl. Mat. 254 (1998) 87–121.
[2] G. Rousseau, L. Desgranges, F. Charlot, N. Millot, J.C. Nièpce, M. Pijolat, F. Valdivieso, G. Baldinozzi, J.F. Berar, J. Nucl. Mat. 355 (2006) 10–20.
[3] L. Desgranges, G. Baldinozzi, G. Rousseau, J.C. Nièpce, G. Calvarin, Inorg. Chem. 48 (2009) 7585–7592.
[4] H. He, D. Shoesmith, Phys. Chem. Chem. Phys. 12 (2010) 8108–8117.
[5] J.M. Elorrieta, L.J. Bonales, N. Rodriguez-Villagra, V.G. Baonza, J. Cobos, Phys. Chem. Chem. Phys. 12 (2016) 8108–8117.
[6] R.I. Cooper, B.T.M. Willis, Acta Cryst. A 60 (2004) 322.
[7] K. Fukuda, J.-S. Choi, R. Shani, L. van den Durpel, E. Bertel, E. Sartori, MOX fuel use as a back-end option: trends, main issues and impacts on fuel cycle management (IAEA-CSP–3/P), Int. At. Energy Agency (IAEA) 31 (49) (2000).
[8] V.J. Tennery, T.G. Godfrey, J. Am. Ceram. Soc. 56 (1973) 129–133.
[9] N.C. Jayadevan, R.G. Hadap, D.M. Chackraburtty, J. Nucl. Mat. 82 (1979) 195–198.
[10] T. Tsuji, M. Iwashita, T. Yamashita, K. Ohuchi, J. Alloys Compd. 271–273 (1998) 391–394.
[11] P. Martin, S. Grandjean, C. Valot, G. Carlot, M. Ripert, P. Blanc, C. Hennig, J. Alloys Compd. 444–445 (2007) 410–414.
[12] R.C. Belin, M. Strach, T. Truphémus, C. Guéneau, J.-C. Richaud, J. Rogez, J. Nucl. Mat. 465 (2015) 407–417.
[13] R. Vauchy, A.-C. Robisson, R.C. Belin, P.M. Martin, A.C. Scheinost, F. Hodaj, J. Nucl. Mat. 465 (2015) 349–357.
[14] J.F. Vigier, P.M. Martin, L. Martel, D. Prieur, A.C. Scheinost, J. Somers, Inorg. Chem. 54 (11) (2015) 5358–5365.
[15] M. Strach, R.C. Belin, J.-C. Richaud, J. Rogez, Inorg. Chem. 53 (2014) 12757–12766.
[16] M. Strach, R.C. Belin, J.-C. Richaud, J. Rogez, J. Phys. Chem.C 119 (40) (2015) 23159–23167.
[17] T. Truphémus, R.C. Belin, J.-C. Richaud, M. Reynaud, M.-A. Martínez, I. Félines, A. Arredondo, A. Miard, T. Dubois, F. Adenot, J. Rogez, J. Nucl. Mat. 432 (2013) 378–387.
[18] C. Jégou, R. Caraballo, J. De Bonfils, V. Broudic, S. Peuget, T. Vercouter, D. Roudil, J. Nucl. Mat. 399 (2010) 68–80.
[19] Z. Talip, S. Peuget, M. Magnin, L. Berardo, C. Valot, R. Vauchy, C. Jégou, J. Raman Spectrosc. 48 (5) (2017) 765–772.
[20] C. Jégou, R. Caraballo, S. Peuget, D. Roudil, L. Desgranges, M. Magnin, J. Nucl. Mat. 405 (2010) 235–243.
[21] C. Jégou, M. Gennisson, S. Peuget, L. Desgranges, G. Guimbretière, M. Magnin, Z. Talip, P. Simon, J. Nucl. Mat. 458 (2015) 343–349.
[22] R. Böhler, M.J. Welland, D. Prieur, P. Cakir, T. Vitova, T. Pruessmann, I. Pidchenko, C. Hennig, C. Guéneau, R.J.M. Konings, D. Manara, J. Nucl. Mat. 448 (2014) 330–339.
[23] L.J. Bonales, J.M. Elorrieta, A. Lobato, J. Cobos, in: Dr Mark Stauffer (Ed.), Raman Spectroscopy, a Useful Tool to Study Nuclear Materials, Applications of Molecular Spectroscopy to Current Research in the Chemical and Biological Sciences, 2016. InTech.
[24] F. Pointurier, O. Marie, Spectrochim. Acta, Part B 65 (2010) 797–804.
[25] E.A. Stefaniak, A. Alsecz, I.E. Sajó, A. Worobiec, Z. Máthé, S. Török, R. Van Grieken, J. Nucl. Mat. 381 (2008) 278–283.
[26] L. Desgranges, G. Baldinozzi, P. Simon, G. Guimbretière, A. Canizares, J. Raman Spectrosc. 43 (2012) 455–458.
[27] G. Guimbretière, L. Desgranges, A. Canizares, G. Carlot, R. Caraballo, C. Jégou, F. Duval, N. Raimboux, M.R. Ammar, P. Simon, Appl. Phys. Lett. 100 (2012) 251914.
[28] D. Ho Mer Lin, D. Manara, P. Lindqvist-Reis, T. Fanghänel, Vib. Spectrosc. 73 (2014) 102–110.
[29] M. Naji, N. Magnani, L.J. Bonales, S. Mastromarino, J.-Y. Colle, J. Cobos, D. Manara, Phys. Rev. B 95 (2017) 104307.
[30] M.J. Sarsfield, R.J. Taylor, C. Puxley, H.M. Steele, J. Nucl. Mat. 427 (2012) 333–342.
[31] M. Naji, J.-Y. Colle, O. Benes, M. Sierig, J. Rautio, P. Lajarge, D. Manara, J. Raman Spectrosc. 46 (2015) 750–756.
[32] F. Lebreton, D. Horlait, R. Caraballo, P.M. Martin, A.C. Scheinost, A. Rossberg, C. Jégou, T. Delahaye, Inorg. Chem. 54 (20) (2015) 9749–9760.
[33] D. Horlait, R. Caraballo, F. Lebreton, C. Jégou, P. Roussel, T. Delahaye, J. Solid State Chem. 217 (2014) 159–168.
[34] M. Chollet, D. Prieur, R. Böhler, R. Belin, D. Manara, J. Chem. Thermodyn. 89 (2015) 27–34.
[35] H. Richter, Z. Wang, L. Ley, Solid State Commun. 39 (1981) 625.
[36] V. Petříček, M. Dušek, L. Palatinus, Z. Krist. 229 (2014) 345–352.
[37] S. Amelinckx, D. van Dyck, J. van Landuyt, G. van Tendeloo, Handbook of Microscopy, Applications in Materials Science, Solid-state Physics and Chemistry, in: Applications, VCH Verlagsgesellschaft mbH, Weinheim, 1997.
[38] T. Wiss, H. Thiele, A. Janssen, D. Papaioannou, V.V. Rondinella, R.J.M. Konings, JOM 64 (2013) 1390–1395.
[39] P.G. Marlow, J.P. Russell, J.R. Hardy, Philos. Mag. 14 (1966) 409–410.
[40] T. Livneh, E. Sterer, Phys. Rev. B 73 (2006) 085118–085119.
[41] G.C. Allen, I.S. Butler, N.A. Tuan, J. Nucl. Mat. 144 (1987) 17–19.
[42] P.R. Graves, Appl. Spectrosc. 144 (1990) 1665–1667.
[43] M.L. Palacios, S.H. Taylor, Appl. Spectrosc. 54 (2000) 1372–1378.
[44] D. Manara, B. Renker, J. Nucl. Mat. 321 (2003) 233–237.

[45] L. Desgranges, G. Guimbretière, P. Simon, C. Jégou, R. Caraballo, Nucl. Instrum. Methods Phys. Res. Sect. B 315 (2013) 169–172.
[46] Q. Yin, S.Y. Savrasov, Phys. Rev. Lett. 100 (2008) 225504.
[47] G. Talsky, Derivative Spectrophotometry: Low and High Order, Verlagsgesellschaft, Weinheim (Federal Republic of Germany) and Inc., New York, NY (USA), 1994.
[48] L. Genzel, T.P. Martin, C.H. Perry, Phys. Stat. Sol. 62 (1974) 83–92.
[49] I.S. Butler, G.C. Allen, N.A. Tuan, Appl. Spectrosc. 42 (5) (1988) 901–902.
[50] G. Leinders, T. Cardinaels, K. Binnemans, M. Verwerft, J. Nucl. Mat. 459 (2015) 135–142.
[51] L. Martel, N. Magnani, J.-F. Vigier, J. Boshoven, C. Selfslag, I. Farnan, J.-C. Griveau, J. Somers, T. Fanghänel, Inorg. Chem. 53 (2014) 6928–6933.
[52] C. Guéneau, A. Chartier, L. Van Brutzel, Compr. Nucl. Mat. 2 (2012) 21–59.